MULTIDISCIPLINARY OPTIMIZATION OF FLEXIBLE WINGS WITH MANOEUVRE LOAD REDUCTION FOR HIGHLY EFFICIENT LONG-HAUL AIRLINERS

T. F. Wunderlich*

* German Aerospace Center (DLR), Institute of Aerodynamics and Flow Technology, Lilienthalplatz 7, 38108 Braunschweig, Germany

Abstract

In the scope of the DLR project oLAF (optimal load-adaptive aircraft), a highly efficient long-haul airliner is being designed, which will be used as a reference for quantifying the potential of active load alleviation. The design of this reference aircraft is based on the technologies of the highly flexible wing, the consideration of basic functions for manoeuvre load reduction and the use of a geared turbofan with a very high bypass ratio. In this work the results of the aero-structural wing optimization will be presented as an essential part of the design work. In this optimization process, high-fidelity simulation methods are used to determine the flight performance in the transonic cruise flight, the loads of the wing in manoeuvre flight and the mass of the wing box made of fibre composite materials. Static aeroelastic effects are considered in all flight conditions and a load reduction due to control surface deflections during manoeuvre flight is taken into account. The minimization of the fuel consumption for three typical flight missions represents the objective function. The geometric integration of the landing gear and the control surfaces, the tailplane sizing and aircraft trimming are considered. The selected design parameters describe the wing planform and the relative profile thickness and twist distribution. The results include a detailed presentation of the optimized wing geometry, the aerodynamic performances in the cruise and manoeuvre flight and the structural mechanical properties after structural sizing.

Keywords

Aero-Structural Design Optimization; Manoeuvre Load Alleviation; Composite Wing

NOMENCLATURE

A	aspect ratio
b	wingspan
c, c_{MAC}	chord, mean aerodynamic chord
g	acceleration of gravity
$n = L/(m\,g)$	load factor
$R = \sum R_i$	range (sum of mission segment ranges)
S	wing area
$t, t/c$	aerofoil and relative aerofoil thickness
x, y, z	coordinates
α	angle of attack
δ	angle of control surface deflection
$\eta = 2y/b$	relative wingspan coordinate

Subscripts

CoG	center of gravity
CWB	center wing box
FS, MS, RS	front spar, middle spar, rear spar
HTP, VTP	horizontal tailplane, vertical tailplane
MG, NG	main gear, nose gear
SL	sea level
WBE	wing fuselage engine configuration

Abbreviations

CO_2	Carbon dioxide
RANS	Reynolds-averaged Navier–Stokes

1. INTRODUCTION

The environmental impact and the need for resources of commercial aviation increases with the growth of global mobility and transport. For environmental protection and conservation of resources the aviation is undergoing a transformation process to energy efficient air transport. This goal is pursued in the DLR's aviation research strategy [1] to support the mobility strategy of the European Green Deal [2]. The main objective for the vehicle is a 25 % reduced fuel consumption of the engines and a 50 % reduction in aircraft energy requirements.

To achieve this challenging goal the development timescales for innovation have to be reduced significantly. In this context the methodologies and processes for physics based aircraft design and optimization have to be improved. Furthermore, an assessment of new technologies based on multidisciplinary optimized configurations under consideration of all relevant disciplines and their interactions on overall aircraft level will be essential in the future.

The efficiency of commercial aircraft is determined by aerodynamic performance in terms of lift to drag ratio, aircraft empty mass and thrust-specific fuel consumption of the engine. For the accurate drag prediction

doi: 10.25967/570055

under cruise flight conditions the flow physics of transonic and viscous flow can be taken into account using RANS-based computational fluid dynamics (CFD). Furthermore, this method enables the prediction of flow separations and the resulting aerodynamic loads under manoeuvre and low speed flight conditions. To reduce the structural mass composite materials like carbon fibre reinforced polymers (CFRP) have been introduced in aircraft manufacturing. The corresponding structural concepts and sizing criteria have to be considered in the structural analysis and sizing process using structural mechanics solvers based on the finite element method (FEM). For further reduction of the thrust-specific fuel consumption of the engine, the technology of geared turbofans enables different rotational speeds of the fan and the low pressure shaft to combine higher bypass ratios with increased component efficiencies.

Within the aero-structural wing optimization the optimum trade-off between the aerodynamic performance and the wing mass is achieved through combining high fidelity methods for numerical flow simulation of the aircraft outer shape and structural sizing of the wing box with an appropriate optimization algorithm. Thereby, the interaction of aerodynamic forces and wing deformations have to be considered for accurate flight performance and static manoeuvre loads prediction using fluid-structure coupling. With increased engine dimensions the integration of the engine is getting more challenging for an underwing arrangement.

Wing design and optimization is a multidisciplinary task with a lot of practical constraints. For example, the size of the tail has to fulfil all stability and control constraints and thus depends on center of gravity range and wing geometry. Furthermore, the landing gear integration, the underwing engine arrangement and the space allocation for the control surfaces including their actuators have to be considered. Neglecting the landing gear integration leads to unrealistic optimization results as shown in [3].

The technology of active manoeuvre load alleviation (MLA) reduces the aerodynamic loads using trailing edge control surface deflections to adapt the lift distribution under manoeuvre flight conditions. This technology has been published by White [4] for example and successfully applied to the Lockheed L-1011 [5]. In modern airliners, the manoeuvre load alleviation functions are an integral part of the flight control system. To reduce the loads due to atmospheric disturbances in flight, active gust load alleviation systems have been developed. An overview of applications of active control technologies for gust load alleviation has been given by Regan and Jutte [6]. The potential of manoeuvre and gust load alleviation to reduce the fuel burn and the direct operating costs has been investigated by Xu and Kroo [7] on aircraft conceptual design level. The active and passive load alleviation technologies have to be integrated into the sizing process of the aircraft structure and result in longer maintenance intervals and mass reductions. Passive load alleviation technologies use specifically designed wing geometries and stiffness characteristics to reduce the loads due to aeroelastic deformations. The anisotropic material properties of carbon fibre reinforced plastics allow improving the aeroelastic behaviour. With the industrial utilisation of automated processes for fibre placements, new technologies in the field of unconventional composites featuring spatially varying tow orientation become possible [8]. Therefore, a physical modelling of active and passive manoeuvre load alleviation technology is pursued in preliminary aircraft design.

With increasing knowledge of composite materials further mass reduction potentials can be exploited by better adaptation of fibre direction to internal loads, introduction of advanced structural concepts, and new manufacturing processes. The more flexible wing concept is a result of mass reduction due to new structural concepts with increased strain allowable and applied to the current generation of aircraft from Boeing (Boeing 787 and Boeing 777-8/9). In addition, the passive load alleviation due to static aeroelastic effects leads to further wing mass reduction. With the increased wing deflections of more flexible wings, the geometric non-linearities affect the internal loads [9] with increased aspect ratio. These geometric non-linearities begin to play a role in current wing design.

The potential of load alleviation technologies has been investigated by Handojo et al. [10] for example. In this work a reduction of the wing box mass up to 27 % could be achieved for a long-haul airliner with unchanged secondary masses and fixed wing planform. The interactions of manoeuvre load alleviation, gust load alleviation and aeroelastic tailoring of the composite wing box structure have been investigated by Binder et al. [11] on the basis of results of different aeroservoelastic optimizations. Thereby, the outer wing shape and the topology of the wing structure have not been optimized and the deflections of the spoilers and ailerons are used for active manoeuvre and gust load alleviation. The results show that 95 % of the maximum achievable mass reduction of a generic long range transport aircraft configuration can be achieved with the combination of manoeuvre load alleviation and aeroelastic tailoring of the wing box structure. In the multidisciplinary wing optimizations published by Wunderlich et al. [12] a significant mass reduction of the optimized wing box is obtained for wings with active manoeuvre load alleviation, resulting in a drop in fuel consumption of about 3 %. Thereby, the wings with active manoeuvre load alleviation results in optimized wing geometries with increased aspect ratio and reduced taper ratio.

Improvements in automation and coupling of accurate simulation methods in combination with advances in numerical optimization strategies lead to the emergence of multidisciplinary design optimization (MDO) based on high fidelity methods. The challenge in using MDO based on high fidelity methods is the large number of design parameters and constraints and the increased computing effort. To overcome this issue, the adjoint method enables the efficient calculation of the

flow variable gradients as a function of the design parameters for gradient-based optimization [13, 14]. Up-to-date applications of the adjoint approach for multidisciplinary wing optimization have been shown in the publications of Kenway and Martins [3]; Liem, Kenway and Martins [15]; Keye et al. [16] and Abu-Zurayk et al. [17]. These publications show that the gradient-based optimization using the adjoint approach is an adequate method for multidisciplinary wing optimization with high fidelity simulation programs and a large number of design parameters.
In this work an iterative approach for wing design and optimization is introduced, which includes overall aircraft design (OAD), aero-structural wing optimization, aerodynamic shape optimization, aircraft system design, loads analysis and aeroelastic design and detailed structural design and sizing. The individual processes are linked by manual interfaces with the support of a central geometry description. With this approach, all relevant disciplines are taken into account in the design process and the required flexibility for engineering decisions is given.

2. DESIGN PROCESS

In the DLR project oLAF the potential for increasing efficiency by the use of active load alleviation technologies is investigated. To quantify this potential, a long haul airliner is designed with today's industrial state of the art load alleviation technologies. The optimal load adaptive aircraft will be designed based on the same top level aircraft requirements (TLARs) and with the same design process under consideration of the extensive use of load alleviation technologies. In FIG. 1 the flow chart of the design process is shown.

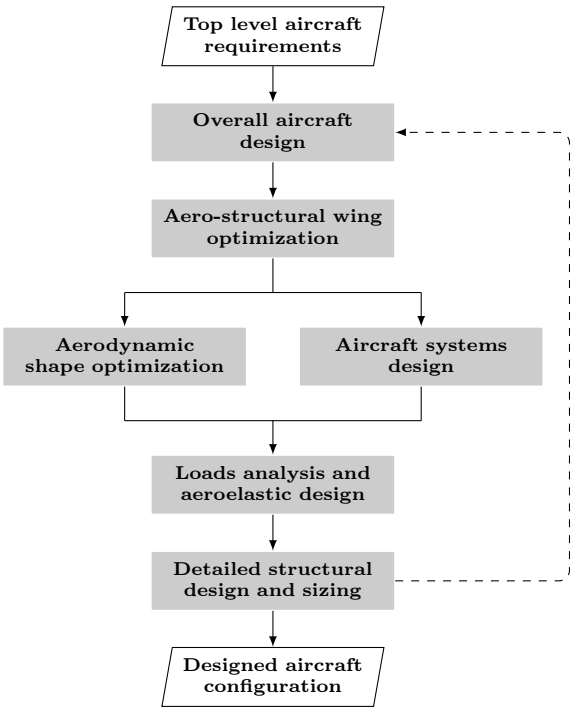

FIG 1. Flow chart of the design process.

The starting point of the design process are the TLARs, which have been defined for a highly efficient long-haul airliner at the beginning of the project. With the overall aircraft design process the wing loading, thrust-to-weight ratio and the resulting aircraft size and masses have been estimated for the given transport task. Thereby, the transport task defines the flight missions in terms of payload, range and flight speeds.
Based on these results an aero-structural wing optimization is executed, to determine the optimal trade-off between aerodynamic cruise flight performance and structural wing mass. In this work the aero-structural wing optimization process and the achieved results for the second design loop under consideration of state of the art load alleviation technologies are presented (see the next sections).
Subsequent to the aero-structural wing optimization the aerodynamic shape optimization and the aircraft systems design are executed in parallel. The optimal aerofoil shapes for a given wing planform are resulting from the aerodynamic shape optimization process. In the aerodynamic shape optimization process a three dimensional gradient-based optimization process based on high fidelity simulation method is used under the consideration of aerofoil thickness constraints. In the aircraft systems design the architecture of the control surface actuation and the flight control systems, which includes the implementation of load alleviation functions are designed.
The loads analysis and aeroelastic design process forms the next step in the design process. Within this process the aircraft loads are computed for the flight envelope. A detailed description of this process and the results for the first design iteration have been published by Schulze et al. [18].
As mentioned before, the individual processes are linked by manual interfaces with the support of the Common Parametric Aircraft Configuration Schema (CPACS) [19, 20]. The result of the design process is the designed aircraft configuration after the iterative process has converged.

3. AERO-STRUCTURAL WING OPTIMIZATION PROCESS

An integrated process for aero-structural wing optimization based on high fidelity simulation methods is continuously developed and improved. A detailed description of the original process chain and their successful application is published by Wunderlich et al. [21, 22]. The improvements relate to the introduction of grid deformation techniques for large geometry changes and simplified control surface deflections. Further extensions include a landing gear integration, a tail sizing based on handbook methods and a trim drag estimation functionality.
The MDO architecture of the integrated process chain falls in the category of MDF optimizations (Multi-Disciplinary Feasible) and can be described as

ASO (Asymmetric Subspace Optimization) according to Martins and Lambe [23].
A detailed description of the process chain is outlined in the publication of Wunderlich et al. [24] and only the top level is presented here again.

3.1. Process chain description

The process chain applied is illustrated in terms of XDSM-diagrams (Extended Design Structure Matrix) [25]. Each component in the diagram receives input data in vertical direction and provides output data in horizontal direction. Input and output data are marked by parallelograms. Thick gray lines show the data flow and thin black arrows indicate the process flow. The numbering system defines the order in which the components are executed.
The flow chart of the process chain for aero-structural wing optimization is shown in FIG. 2. In every optimization step, the geometrical aircraft description of the baseline configuration is recalculated and updated in accordance with the current values of the design parameters. The resulting aircraft geometry is transferred to the subsequent simulation programs using CPACS. The recalculation of the aircraft geometry includes the wing positioning relative to the fuselage, the integration of the main landing gear, the sizing of the tail and the check of geometrical constraints.
In the next step the parametric CAD model is updated, the aerodynamic volume mesh is deformed, and the structural model is generated. The parametric CAD model has been built in the commercial software CATIA® V5, which enables accurate surface representation and robust and time efficient geometry changes. Within the CFD volume mesh deformation process, the mesh representing the baseline configuration is deformed in two stages for all flight conditions in parallel. In the first stage, the geometrical changes between the baseline and the current geometry are computed based on the corresponding structured multiblock (SMB) surface meshes. The latter result from the automatic surface mesh generation and have an identical mesh topology with the same number of points. For automatic surface mesh generation, the commercial software Pointwise® is applied. In the second stage, the control surface deflections are taken into account. Corresponding to the control surface deflection to be produced, the surface mesh displacement field is computed for each flight condition. It is propagated to the CFD volume mesh using the Elasticity Analogy (EA) mesh deformation method [26] available in the FlowSimulator [27–29] environment.
For the generation of the structural model the DLR in-house tool DELiS (Design Environment for thin-walled Lightweight Structures) [30] is used. Based on the central data format CPACS, DELiS automatically generates a consistent finite element mesh using the open-source tool Gmsh [31]. The finite element model is made up of shells elements enriched with physical properties of the wing spars, ribs and skin cells and finally exported for the commercial FE solver MSC Nastran™.
The fluid-structure coupling loop is marked with a rounded yellow box and the values of the design mission lift-to-drag ratio, the wing mass and the objective function value are evaluated for the convergence examination. The fluid-structure interaction belongs to the category of loosely coupled analysis [32, 33], with the main difference of replacing the structural analysis of a sized wing structure by a combined structural wing analysis and sizing process. The integration of the structural sizing process into the fluid-structure coupling loop reduces the number of iterations by introducing a damper like behaviour.
For all flight conditions the aerodynamic forces and coefficients are computed using RANS-based CFD simulations. The flow simulations are performed using the DLR TAU-Code [34, 35] which is integrated in the HPC framework FlowSimulator [27]. The solver's capabilities with respect to accurate flow predictions, also in near off-design regions, have been demonstrated in numerous publications, including those of the AIAA Drag Prediction Workshop Series [36]. The approach ensures that flight performance under cruise flight conditions and selected manoeuvre loads with consideration of flow separations in the presence of control surface deflections are analysed accurately and efficiently.
Based on the aerodynamic loads computed for the flight conditions considered, the wing-box structure is sized. Within the structural analysis and sizing process the objective is to fulfil the structural constraints in terms of failure criteria and converge the margins of safety (MoS) and wing mass. Hence, the structural analysis and sizing process represents a subspace optimization, which is described in detail in the publication of Wunderlich et al. [24]. Different design criteria are applied to ensure a valid structural design. As proposed by Dähne et al. [37] for stiffened panels, the criteria for strength, maximum strain and local and global buckling are used for skin and all stringer components. The main results of this process are the wing mass and the deformed wing shapes for the flight conditions considered. The structural analysis and sizing process uses the linear analysis of the commercial software MSC Nastran™ for computing the internal loads and stresses. The commercial software HyperSizer® is applied for sizing the composite wing box.
The structural deformations form the input for the CFD volume mesh deformation. The mesh deformation method based on radial basis functions (RBF) [38] available in the FlowSimulator is used. Afterwards, the objective function is evaluated and the convergence criteria of the static aeroelastic analysis are examined. Once convergence of the fluid-structure coupling loop is reached, the objective function value is given to the global optimizer.
After the optimization run has finished the optimized vector of design parameters represents the main result of the process chain for the corresponding optimization problem.

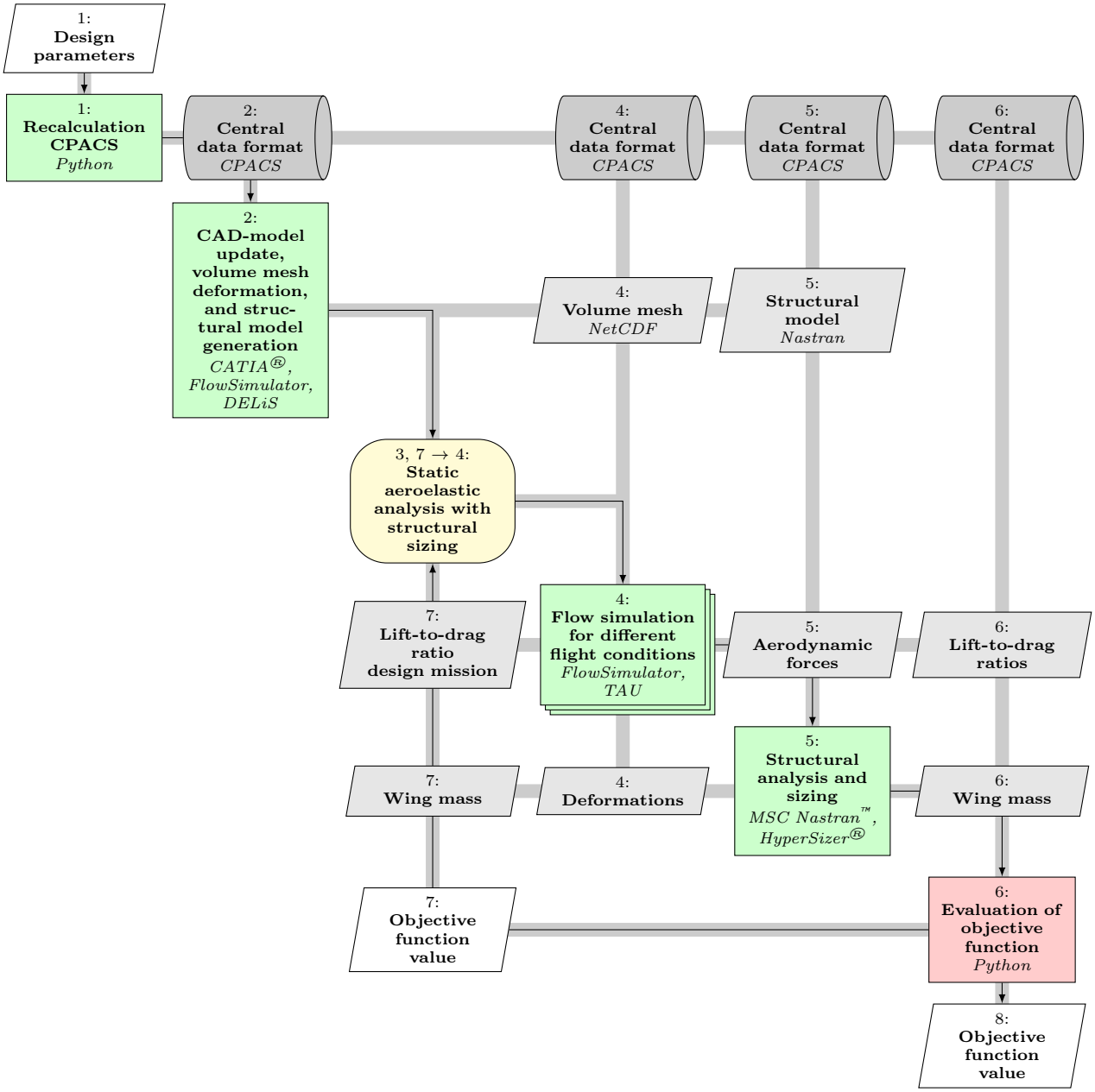

FIG 2. Flow chart of the process chain for aero-structural wing optimization.

3.2. Global optimization strategy

For the wing optimizations in this work an in-house surrogate-based optimization (SBO) method implemented by Wilke [39] has been selected. This global optimization strategy represents an adequate compromise between exploring the design space and locating the optimum.

The selected optimization method is an implementation of the optimization method EGO (Efficient Global Optimizer), which has been introduced by Jones et al. [40] and is discussed in Forrester et al. [41]. At the beginning of the optimization a design of experiments (DoE) for a selected number of samples is performed. In this work, the central Voronoi tessellated (CVT) Latin hypercube [42] has been selected as primary DoE technique. For the calculated objective function value and for each selected constraint, a surrogate model based on kriging [43] is built. These surrogate models are able to model the non-linear behaviour of the objective and constraints. Additionally, a statistical error estimation is included.

Based on the surrogate models of the objective function and constraints, a hybrid optimization strategy is used to find the optimum in terms of expected improvement (EI), which combines the predictions of objective function value and model error. The hybrid optimization strategy starts with a global optimization method and the localization of the optimum is improved by the application of a local optimization method. For the global optimization the differential evolutionary (DE) algorithm published by Storn and Price [44] is used. The simplex pattern search method from Nelder and Mead [45] has been selected for the local search in the surrogate models. For the resulting global optimum in terms of expected improvement

			Study mission	High speed mission	Design mission
Flight missions	Weight factor	w_i	0.6	0.1	0.3
	Cruise Mach number	Ma	0.83	0.85	0.83
	Range	R	4000 nm (7408 km)	4000 nm (7408 km)	6000 nm (11 112 km)
	Payload	m_P	40 800 kg	40 800 kg	variable, see TAB. 3
	Reserve fuel ratio	$m_{F,res}/m_F$	0.14	0.14	0.10

TAB 1. Flight missions.

a recalculation with the physical model is performed. The result of this recalculation is then used to improve the surrogate models for the objective function value and constraints. The described optimization procedure is iterated until convergence is reached.

4. MULTI-MISSION AERO-STRUCTURAL WING OPTIMIZATION

In the DLR project oLAF multi-mission aero-structural wing optimizations have been successfully applied to optimize wing planform, twist and thickness distribution of the baseline configuration. The baseline aircraft represents a conventional twin-engine wide-body aircraft configuration of a long-haul airliner. The fuselage cross-section is elliptical and the wing is arranged as a low-wing aircraft. For the propulsion a new generation geared turbofan has been selected. The large engines are positioned in underwing configuration and the main landing gear is attached to the wing.
In the first iteration loop of the design process the shapes of the fuselage and the belly fairing have been designed. Furthermore, the engine outer dimensions have been adapted to the engine design, which has been contributed by the DLR-Institute of Propulsion Technology. The introduced process for aero-structural wing optimization has been successfully applied to optimize the toe-in angle of the through-flow nacelle. The results of the first iteration loop are not presented here.
In the second iteration loop of the design process the aero-structural wing optimization has been repeatedly executed with additional consideration of basic functions for manoeuvre load alleviation and of a touch-down manoeuvre load case in the structural sizing of the wing box. The results obtained are presented in detail in this section.

4.1. Design task

The design task describes the objective function, the design space and the constraints. In this work, the wing design for a highly efficient long-haul airliner has been performed.

4.1.1. Objective function, flight missions and load cases

The objective function of the multi-mission aero-structural wing optimization is the combined fuel consumption of three selected flight missions. In this work, the fuel consumption is defined in terms of fuel burn per range and payload. Hence, the combined fuel consumption is the weighted sum of the corresponding mission fuel consumption as given in Eq. (1).

$$\frac{m_F}{R\, m_P} = \sum_i w_i \left(\frac{m_F}{R\, m_P} \right)_i \tag{1}$$

In TAB. 1 an overview of the selected flight missions and weighting factors is shown. With the selected weighting factors the expected relative frequency of the missions in operation has been considered.
For the study and design mission the design Mach number of the Airbus A330 has been selected. The design mission range is set to 6000 nm and the corresponding payload is a result of the aero-structural wing analysis. The selection of range and payload for the study mission is based on a typical long range mission with a passenger load factor of 0.85 and represents the mission for which the aircraft will be optimized primarily. The difference between high speed and the study mission is the increased cruise Mach number to consider off-design conditions in the wing optimization.
To compute the fuel consumption of each flight mission a modelling from conceptual design [46, 47] has been used. Thereby, the flight mission has been divided into five segments and the corresponding aircraft mass fractions have been transferred from typical values given in the textbook published by Jenkinson [48] to the baseline aircraft configuration. The flight mission segments are summarized in TAB. 2.

Segment number	Mission segment	Aircraft mass fraction [48]
1	Taxi and take-off	$m_1/m_{TO} = 0.997$
2	Climb and accelerate	$m_2/m_1 = 0.981$
3	Cruise	Eq. (3)
4	Descent for landing	$m_4/m_3 = 0.998$
5	Landing and taxi	$m_5/m_4 = 0.997$

TAB 2. Flight mission segments.

For the cruise segment of the flight mission a constant Mach number and constant lift-to-drag ratio have been assumed. Furthermore, the thrust-specific fuel consumption has been modelled by a formula published by Mattingly [49]. This formula describes the dependency of the thrust-specific fuel consumption from the flight conditions for a given engine and has been adapted to the engine map of a geared turbofan provided by the

DLR-Institute of Propulsion Technology. The formula with the adopted parameters are given in Eq. (2).

$$TSFC = \frac{C_1 + C_2 Ma}{g}\sqrt{\frac{\theta}{\theta_{SL}}} \quad \text{with } C_1 = 0.216\,\mathrm{h}^{-1} \text{ and } C_2 = 0.415\,\mathrm{h}^{-1} \tag{2}$$

The aircraft mass fraction for the cruise segment is calculated with Eq. (3), which has been derived from the well-known Breguet range equation and the thrust-specific fuel consumption of Eq. (2).

$$R_{23} = a_{SL}\,\frac{Ma}{C_1 + C_2\,Ma}\,\frac{L}{D}\,\ln\frac{m_2}{m_3} \quad \text{with } a_{SL} = \sqrt{\kappa\,R\,\theta_{SL}} = 340.3\,\mathrm{m/s} \tag{3}$$

For each flight mission the corresponding lift-to-drag ratio for the cruise segment is approximately the result of the aerodynamic coefficients of the flow simulation for the wing body engine configuration, the estimated aerodynamic coefficients of the tail and the given residual drag and residual thrust coefficients as shown in Eq. (4).

$$\frac{L}{D} \approx \frac{\overbrace{C_{L,WBE}}^{\text{flow simulation}} + C_{L,HTP}}{\underbrace{C_{D,WBE}}_{\text{flow simulation}} + C_{D,HTP} + C_{D,VTP} + \Delta C_D} \quad \text{with } \Delta C_D = C_{D,res} - C_{T,res} \tag{4}$$

The lift coefficient of the horizontal tail is a result of aircraft trimming for the prescribed center of gravity position. This aircraft trimming loop based on the equilibrium of forces and moments around the center of gravity and provides the accurate value for the engine thrust and the resulting lift-to-drag ratio. This trimming loop and the corresponding equations are not described in detail here. For the drag coefficient prediction of the tail a simplified approach from conceptual design [50] based on Prandtl's lifting-line theory and flat plate analogy has been used.
The take-off mass of the aircraft is the sum of the residual mass m_{Res} (structural mass without the wing and tail including the operating items mass), the wing mass m_W, the tail mass, the payload and the fuel masses (mission and reserve fuel) as shown in Eq. (5).

$$m_{TO} = \overbrace{m_{Res} + m_W + m_{HTP} + m_{VTP}}^{\text{operating empty mass } m_{OE}} + m_P + m_F + m_{F,res} \tag{5}$$

The wing mass is a result of the structural sizing of the wing box and the tail mass is estimated by scaling the tail mass of the reference aircraft with the tail surface ratio after tail sizing. Thereby, the tail sizing based on conceptual design methods using constant tail volume coefficients [51]. The fuel mass follows directly from the aircraft mass difference for the complete flight mission.
For the calculation of the fuel consumption, the required equations are listed in TAB. 3. Thereby, the fuel mass ratio m_F/m_{TO} is computed from the aircraft mass fractions with the given range R and the lift-to-drag ratio L/D for the cruise segment. For the study mission and the high speed mission, the payload is specified and the take-off mass has to be calculated. In the design mission the take-off mass equals the maximum take-off mass and the payload is resulting from the cruise flight performance and wing mass. For both cases, the corresponding equations are evaluated in terms of the payload ratio m_P/m_{TO}. With the fuel mass ratio and the payload ratio the fuel consumption per range and payload follows directly from the last equation in TAB. 3.

Fuel mass ratio	$\frac{m_F}{m_{TO}} = 1 - \frac{m_1}{m_0}\frac{m_2}{m_1}\frac{m_3}{m_2}\frac{m_4}{m_3}\frac{m_5}{m_4}$
Payload ratio	For specified m_{TO} and variable m_P: $\frac{m_P}{m_{TO}} = 1 - \frac{m_{OE}}{m_{TO}} - \left(1 + \frac{m_{F,res}}{m_F}\right)\frac{m_F}{m_{TO}}$ For specified m_P and variable m_{TO}: $\frac{m_P}{m_{TO}} = \frac{1 - \left(1 + \frac{m_{F,res}}{m_F}\right)\frac{m_F}{m_{TO}}}{m_{OE} + m_P} m_P$
Fuel consumption	$\frac{m_F}{R\,m_P} = \frac{m_F}{m_{TO}}\frac{m_{TO}}{m_P}\frac{1}{R_{12}+R_{23}+R_{34}}$

TAB 3. Used formulas for the computation of the fuel consumption.

To evaluate the fuel consumption for the given flight missions the flow simulation are executed for three flight cases. Based on these flight cases, the lift-to-drag ratios are calculated with the assumptions described before. In TAB. 4 the selected flight cases for the aerodynamic cruise flight performance computation are given.
For the structural sizing of the wing box, the manoeuvre load cases with the maximum loads have to be defined. These manoeuvre load cases have been derived from the flight envelope limits and the limits of the manoeuvring load factor resulting from the certification regulations CS-25/FAR 25. In TAB. 4 an overview of the selected manoeuvre load cases is given.

4.1.2. Design parameters and constraints

The outer shape of the wing has been parameterized with the design parameters shown in FIG. 3.
Thereby, the wing planform is calculated from wing area, aspect ratio, position of inboard and outboard kink, inboard and outboard leading edge sweep angle, and the taper ratios of the inboard, mid wing and outboard wing region. Furthermore, the twist and relative thickness distribution are defined in the corresponding wing sections. In the wing sections between these sections the values of the twist and relative thickness are interpolated linearly or optionally with the usage of a spline interpolation. The fuselage shape has been held constant during the wing optimizations. For the

	Name	Mach number Ma	Altitude H	Mass m	Load factor n_z	Aircraft settings
Flight cases	FC1	0.83	10 668 m	190 389 kg	1.0	Cruise configuration
	FC2	0.85	10 668 m	192 550 kg	1.0	Cruise configuration
	FC3	0.83	10 363 m	203 367 kg	1.0	Cruise configuration
Load cases	LC1	0.552	0 m	221 078 kg	+2.5	$\delta_{ail,in} = -10°$, $\delta_{ail,out} = -15°$
	LC2	0.655	3048 m	222 760 kg	−1.0	$\delta_{ail,in} = 5°$, $\delta_{ail,out} = 10°$
	LC3	0.552	0 m	219 952 kg	+2.0	$\delta_{flap,out} = 10°$, $\delta_{ail,in} = 5°$
	LC4	0.265	0 m	187 081 kg	-	High-lift configuration

TAB 4. Flight cases and load cases.

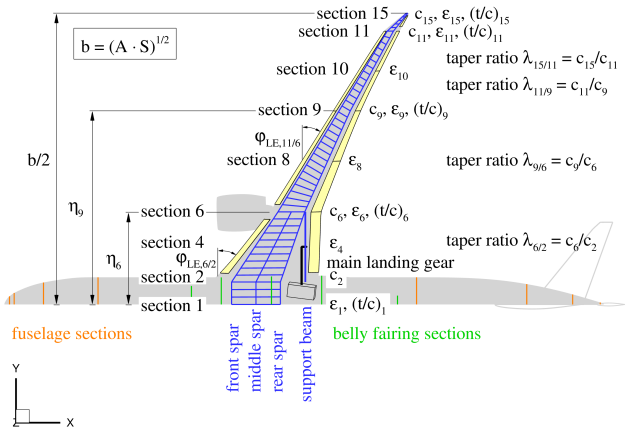

FIG 3. Outer shape design parameters.

belly fairing an adaptation to the root section of the wing has been considered by scaling the middle section of the belly fairing. The positioning of the wing in x-direction has been performed by maintaining the x-position of the aerodynamic center.

The wing box regions and the topology are shown in FIG. 4.

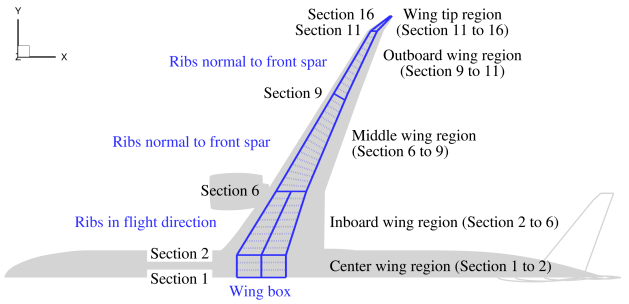

FIG 4. Wing box regions and topology.

Thereby, the wing box has been separated into five regions. The definition of the spars is based on the relative positioning of spar points, which are given in relative span and relative chord coordinates. For the ribs a constant rib spacing for each wing region has been considered. In the center wing, inboard and wing tip region the ribs are oriented in flight direction and in the middle and outboard wing region the ribs are positioned normal to the front spar. These rib orientations are typical for Airbus aircraft. For the covers, spars and ribs the percentage ply share has been defined in the five selected wing box regions. All selected values are given in section 4.3.

The definition of the control surfaces is shown in FIG. 3. For the consideration of the active manoeuvre load alleviation the deflections of the inboard flap, outboard flap and outboard aileron have been defined for the load cases and given in TAB. 4.

During the wing optimization the required fuel tank volume is calculated for all selected flight missions and compared with the useable fuel tank volume. The fuel tank volume constraint has been considered in all wing optimizations.

With the consideration of geometry constraints for the integration of a landing gear and the control surfaces, a better comparability of the optimization results with the baseline aircraft configuration is achieved. FIG. 5 gives an overview of the geometrical constraints, which have to be fulfilled for each wing design.

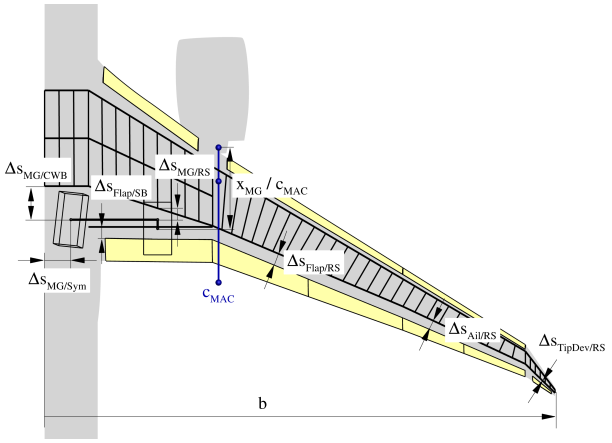

FIG 5. Geometrical constraints.

This includes the positioning of the main gear wheel on the ground with a given relative x-position while maintaining the minimal allowed distances between the main landing gear, the control surfaces and the wing box.

In FIG. 6 further geometrical constraints for the landing gear integration are shown. For each aircraft category the outer main gear wheel span has to be within

the given limits. Furthermore, the geometrical constraints for nose down engine clearance h_{NDEC}, touch down tail clearance h_{TC}, and engine and wing clearances h_{EC}, h_{WC} for a bank angle of $\varphi = 7°$ have to be fulfilled. The selected values are given in TAB. 6.

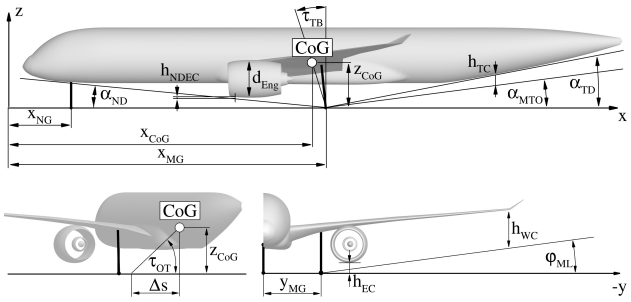

FIG 6. Landing gear constraints.

The introduced landing gear integration consists of a design loop for automatic positioning. Thereby, the main gear wing attachment point is shifted from inboard to outboard position and from front to rear position for each span location. All geometrical constraints are checked for each prescribed position, until a feasible design is found.
In TAB. 5 the introduced design parameters are summarized. The design parameters include wing planform and wing section parameters.

Wing area	S
Aspect ratio	A
Inboard kink position	η_6
Outboard kink position	η_{11}
Taper ratio inboard	$\lambda_{6/2}$
Taper ratio mid wing	$\lambda_{9/6}$
Taper ratio outboard	$\lambda_{11/9}$
Inboard leading edge sweep angle	$\varphi_{LE,6/2}$
Outboard leading edge sweep angle	$\varphi_{LE,11/6}$
Twist distribution	ε_1, ε_6, ε_8, ε_9, ε_{11}, ε_{15}
Relative thickness distribution	$(t/c)_1$, $(t/c)_6$, $(t/c)_9$
Relative main landing gear position	x_{MG}/c_{MAC}

TAB 5. Design parameters.

The constraints consist of mass constraints, propulsion constraints, geometrical constraints for airport conformity, landing gear and control surface integration constraints, flight mission constraints and structural sizing constraints. In TAB. 6 the used values and their limits are given.

4.2. Manoeuvre load reduction

The active manoeuvre load alleviation (MLA) reduces the aerodynamic loads using trailing edge control surface deflections to adapt the lift distribution under manoeuvre flight conditions. In a pull up manoeuvre for example, an inboard load shift can be achieved by increasing the lift in the inboard region with positive control surface deflections and decreasing the lift in the outboard wing region with negative control surface deflections. The result of the inboard load shift are reduced aerodynamic loads in terms of wing bending moment. Thereby, the inboard load shift is related to a forward shifting of the center of pressure in the case of backward swept wings and the aircraft trimming redistributes the lift between the wing and the horizontal tail. As a result, the lift of the horizontal tail increases and simultaneously the lift of the wing decreases.
The aerodynamic limits of the lift distribution adaptation are the minimum and maximum local lift coefficients with deflected control surfaces. These limits can be explained with flow separations in viscous flow. Furthermore, the geometrical extension of the control surfaces are limited by the rear spar position of the wing box and the required actuator size, mass and actuation power.
In this work the control surface deflections are modelled using a mesh deformation approach. This ap-

Maximum take-off mass	$m_{MTO} = 220\,000\,\mathrm{kg}$
Maximum payload	$m_{P,max} = 54\,000\,\mathrm{kg}$
Residual mass ratio	$m_{Res}/m_{MTO} = 0.3952$
Specific mass of leading edge	$m_{LE}/S_{LE} = 30\,\mathrm{kg/m^2}$
Specific mass of trailing edge	$m_{TE}/S_{TE} = 50\,\mathrm{kg/m^2}$
Wingspan (FAA Group V and ICAO Code E)	$52\,\mathrm{m} \leq b \leq 65\,\mathrm{m}$
Fuel tank volume	$V_F \geq V_{F,req}$
Outer main gear wheel span (ICAO Code E)	$9\,\mathrm{m} \leq 2\,y_{MG} \leq 14\,\mathrm{m}$
Nose gear static load ratio	$5\,\% \leq F_{NG}/m\,g \leq 20\,\%$
Tip back angle	$\tau_{TB} \geq 15°$
Overturn angle	$\tau_{OT} \leq 63°$
Take-off rotation angle (with 0.25 m tail clearance)	$\alpha_{TO} \geq 10°$
Tail down angle	$\alpha_{TD} \geq 11°$
Tail clearance	$h_{TC} \geq 0.25\,\mathrm{m}$
Wing and engine clearance (with 7° bank angle)	$h_{WC},\ h_{EC} \geq 0.4\,\mathrm{m}$
Nose down engine clearance	$h_{NDEC} \geq 0.1\,\mathrm{m}$
Castor angle of main gear leg	$83° \leq \tau_{Cas} \leq 90°$
Distance between main gear and wing box	$1.9\,\mathrm{m} \leq \Delta s_{MG/CWB} \leq 2.9\,\mathrm{m}$
Distance between main gear and symmetry plane	$1.4\,\mathrm{m} \leq \Delta s_{MG/Sym} \leq 1.6\,\mathrm{m}$
Distance between main gear and rear spar	$0.6\,\mathrm{m} \leq \Delta s_{MG/RS} \leq 1.6\,\mathrm{m}$
Distance between flap and support beam	$\Delta s_{Flap/SB} \geq 0.2\,\mathrm{m}$
Distance between flap and rear spar	$\Delta s_{Flap/RS} \geq 0.065\ c_{MAC}$
Distance between aileron and rear spar	$\Delta s_{Ail/RS} \geq 0.04\ c_{MAC}$
Distance between tip device and rear spar	$\Delta s_{TipDev/RS} \geq 0.01\ c_{MAC}$
Residual drag coefficient	$C_{D,res} = 0.0018$
Residual thrust coefficient (through-flow nacelle)	$C_{T,res} = 0.0030$

TAB 6. Constraints.

proach allows for the consideration of viscous flow effects including flow separations in the aerodynamic loads computation, but neglects the complex flow physics around the edges of the deflected control surfaces.

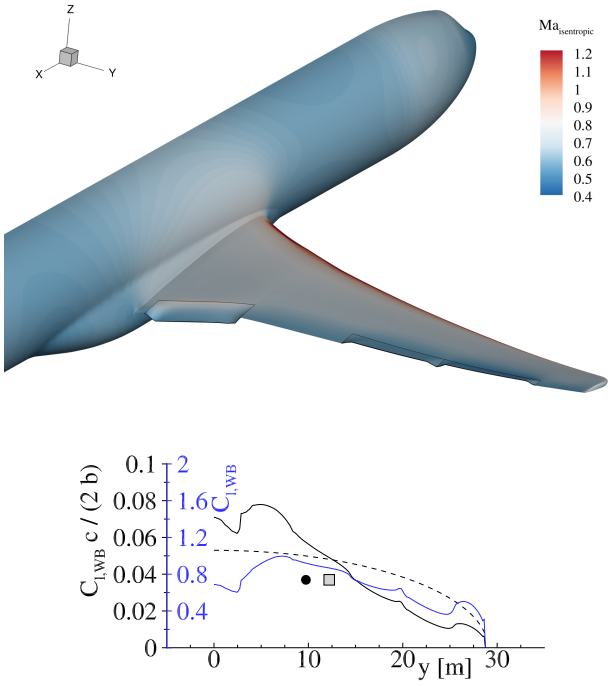

FIG 7. Manoeuvre load alleviation.

In FIG. 7 the surface solution for a pull up manoeuvre with control surface deflections for active manoeuvre load alleviation is shown. The corresponding lift- and lift coefficient distribution with the center of lift (black dot) are presented on the right side of the figure. Furthermore, the elliptical lift distribution (dashed line) with its center of lift (gray square) is shown as reference.
In this work the wing design of the baseline aircraft configuration with basic functions for manoeuvre load alleviation is introduced. This basis functions uses the ailerons with prescribed limits for the deflection angles. In TAB. 4 the prescribed control surface deflections are given for manoeuvre load alleviation of the considered load cases.
With the introduction of more aggressive manoeuvre load alleviation in the second project phase further wing box mass reduction and fuel consumption reduction will be expected.

4.3. Structural concept

For the composite wing structure of the baseline aircraft configuration a conventional structural concept with relaxed strain allowables is used. With this approach a proven structural concept for a realistic wing box structure has been selected, which takes the concept of more flexible wing into account.

The structural concept with a fixed standard ply share has been summarized in TAB. 7 for the baseline aircraft configuration.

Stringer type	I-stringer	
Strain allowable	Tension	4000 µm/m
	Compression	3500 µm/m
	Shear	8000 µm/m
Ribs spacing Δs_{Rib}	Center wing	0.85 m
	Inboard wing	0.85 m
	Middle wing	0.75 m
	Outboard wing	0.75 m
	Wing tip	0.50 m
Percentage ply share covers 0°/ ± 45°/90°	Center wing	70/20/10
	Inboard wing	40/50/10
	Middle wing	40/50/10
	Outboard wing	30/60/10
	Wing tip	30/60/10
Percentage ply share spars 0°/ ± 45°/90°	Complete wing	50/40/10
Percentage ply share ribs 0°/ ± 45°/90°	Complete wing	40/50/10

TAB 7. Structural concept overview.

With the usage of I-stringers the stiffness of the covers is reduced and the increased damage tolerance allows the relaxation of the strain allowables in comparison to a conventional structure with T-stringers. For this reason the conservative value of the strain allowable has been relaxed from 3500 µm/m as proposed in Military Handbook [52] to the value of 4000 µm/m.
The selected ribs spacing results from the required man holes in the lower cover of the wing box for safety checks and maintenance.

4.4. Wing optimization results

In this section the wing optimization results are presented. Based on the baseline aircraft geometry, wing planform including the twist and thickness distribution have been optimized with prescribed aerofoil shapes resulting from the aerodynamic shape optimization process as described before.
In the next step the optimized wing has been recalculated with modified aerofoil shapes in the middle and outboard wing region to improve low speed aerodynamics. This recalculation uses the spline interpolation of the twist and relative thickness distribution and smooth leading and trailing edge curves in comparison to the wing optimization.
The resulting wing geometries are presented in FIG. 8 and the corresponding twist and thickness distributions are shown in FIG. 9. Thereby, the wing planform, the wing box geometry with the spars and ribs, the landing gear including the support beam and the control surface geometries are presented. The twist distribution for the rigid “jig-shape” and the elastic “flight-shape” are shown for the wings. The shown “flight-shape” results from the wing deformations at

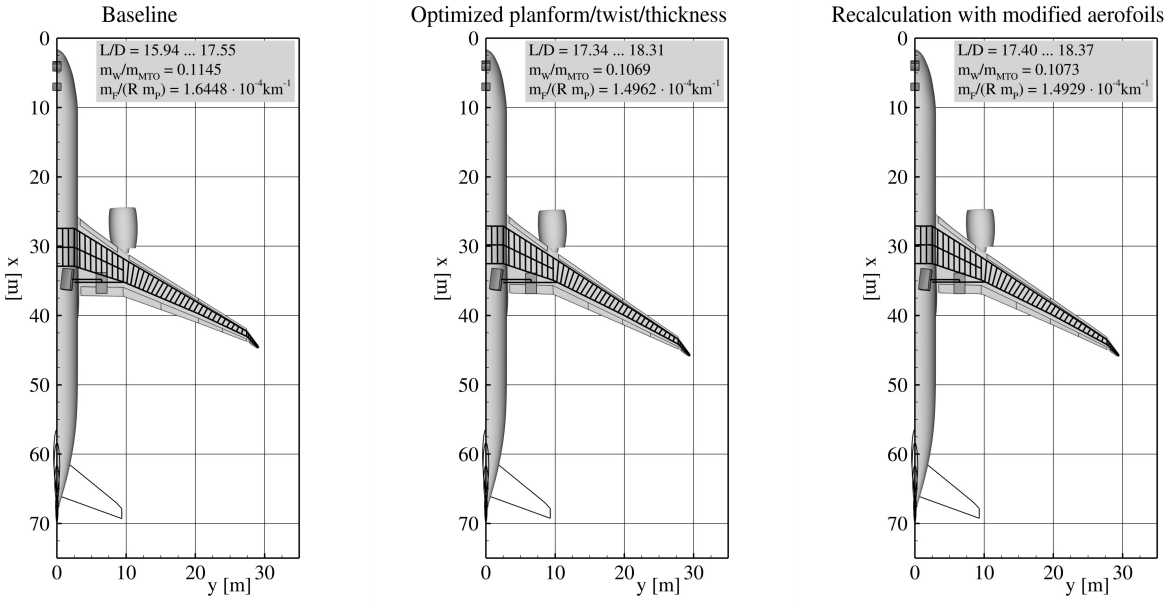

FIG 8. Wing planforms with structure layout of wing optimizations with different aerofoils.

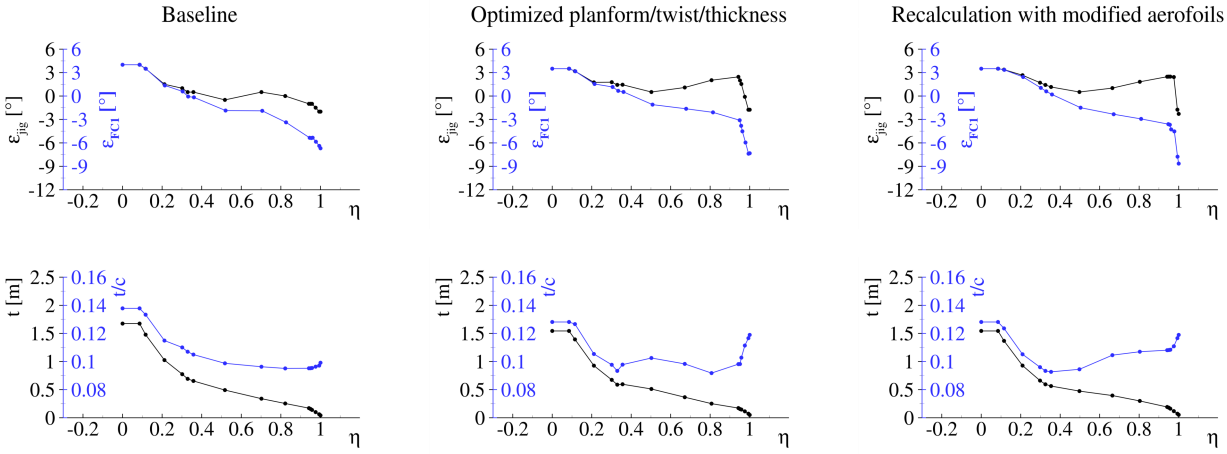

FIG 9. Twist- and thickness distributions of wing optimization with different aerofoils.

the beginning of the "study mission", which have been simulated with flight case "FC1" (see TAB. 4). For the structural interpretation of the results, the absolute wing thickness distribution is given. In addition, the relative thickness distribution for the aerodynamic interpretation is presented.

The results of the wing optimization show a wing with significant thin inboard wing sections. With the aero-structural wing optimization an optimal trade-off between cruise flight performance and wing mass in terms of combined fuel consumption has been achieved. In TAB. 8 an overview of all relevant values is given. A value lower than one of the used fuel tank volume for the design mission indicates that the fuel volume constraint is fulfilled. The results of the wing optimization show slightly reduced wing area, increased wingspan and higher leading edge sweep angles. This leads to increased transonic cruise flight performance without drawbacks due to wing mass changes.

The introduction of basic functions for manoeuvre alleviation results in significant mass reduction of the optimized wing. The cruise flight performance improvements in terms of lift-to-drag ratio result from the wing planform, twist and thickness optimization and in addition from the adapted aerofoil shapes. In comparison to the baseline aircraft configuration the optimized wing show a fuel consumption reduction in the order of 9 %.

In FIG. 10 and FIG. 11 an overview of the aerodynamic results is given for the cruise flight condition. For each lift distribution in FIG. 10 the related elliptical lift distribution is shown by a dashed dotted line and the corresponding center of lift is indicated by a white rectangle as a reference. The elliptical lift distribution is optimum for planar wings in terms of lift induced drag. For the cruise flight condition the results of the planform, twist and thickness optimization show a nearly elliptical lift distribution. The corresponding center of lift is indicated by a black circle. This leads in

			Baseline	Optimized planform, twist and thickness	Recalculation with modified aerofoils
Wing Geometry	Wing area	S_W	338.5 m^2	337.0 m^2	337.0 m^2
	Wingspan	b_W	58.18 m	58.86 m	58.86 m
	Mean aerodynamic chord	$c_{MAC,W}$	7.69 m	7.60 m	7.59 m
	Aspect ratio	A_W	10.001	10.281	10.280
	Taper ratio	λ_W	0.036	0.035	0.036
	Leading edge sweep angle	$\varphi_{W,LE,6/2}$	36.0°	36.6°	36.6°
		$\varphi_{W,LE,11/6}$	32.0°	34.5°	34.5°
	Flap spar offset	$\Delta s_{Flap/RS}$	0.58 m	0.60 m	0.61 m
	Aileron spar offset	$\Delta s_{Ail/RS}$	0.33 m	0.31 m	0.31 m
	Useable fuel tank volume	V_F	115.68 m^3	107.60 m^3	105.97 m^3
Tail geometry	Horizontal tail area	S_{HTP}	70.2 m^2	69.0 m^2	69.0 m^2
	Vertical tail area	S_{VTP}	49.0 m^2	49.3 m^2	49.3 m^2
Landing Gear	Landing gear wheel base	l_{LG}	28.29 m	28.36 m	28.35 m
	Outer main gear wheel span	$2\,y_{MG}$	12.88 m	13.03 m	12.87 m
	Nose gear static load factor	$F_{NG}/(m\,g)$	$0.054, \ldots, 0.076$	$0.057, \ldots, 0.078$	$0.057, \ldots, 0.078$
	Tipback angle	τ_{TB}	$17.0°, \ldots, 23.6°$	$17.5°, \ldots, 23.9°$	$17.5°, \ldots, 23.8°$
	Overturn angle	τ_{OT}	$40.2°, \ldots, 40.3°$	$40.5°, \ldots, 40.6°$	$40.9°, \ldots, 41.0°$
	Tail down angle	α_{TD}	11.2°	11.4°	11.5°
	Main gear spar offset	$\Delta s_{MG/RS}$	0.65 m	0.95 m	1.00 m
	Main gear flap offset	$\Delta s_{Flap/SB}$	0.64 m	0.26 m	0.28 m
Masses	Mass of covers	$m_{W,covers}$	8378 kg	7604 kg	7718 kg
	Mass of spars	$m_{W,spars}$	2590 kg	2414 kg	2440 kg
	Mass of ribs	$m_{W,ribs}$	2402 kg	2012 kg	1928 kg
	Wing box mass[a]	$m_{W,box}$	16 713 kg	15 038 kg	15 108 kg
	Operat. empty mass ratio	m_{OE}/m_{MTO}	0.5265	0.5188	0.5192
	Wing mass ratio	m_W/m_{MTO}	0.1145	0.1069	0.1073
Manoeuvre n=2.5	Manoeuvre load alleviation	-	no	basic functions (ailerons)	basic functions (ailerons)
	Angle of attack	α	6.9°	9.5°	7.3°
	Lift-to-drag ratio	L/D	19.43	8.04	16.87
	Center of pressure	$y_{CoP}/(b/2)$	0.3663	0.3256	0.3438
	Inboard aileron deflection	$\delta_{ail,in}$	0.0°	−10.0°	−10.0°
	Outboard aileron deflection	$\delta_{ail,out}$	0.0°	−15.0°	−15.0°
Study mission	Angle of attack	α	2.7°	2.9°	2.4°
	Lift-to-drag ratio	L/D	17.44	18.22	18.25
	Center of pressure	$y_{CoP}/(b/2)$	0.3898	0.3884	0.3934
	Fuel consumption	$m_F/(R\,m_P)$	1.501×10^{-4} km^{-1}	1.418×10^{-4} km^{-1}	1.417×10^{-4} km^{-1}
High speed mission	Angle of attack	α	2.4°	2.5°	2.1°
	Lift-to-drag ratio	L/D	15.94	17.34	17.40
	Center of pressure	$y_{CoP}/(b/2)$	0.3851	0.3875	0.3920
	Fuel consumption	$m_F/(R\,m_P)$	1.634×10^{-4} km^{-1}	1.479×10^{-4} km^{-1}	1.474×10^{-4} km^{-1}
Design mission	Payload	m_P	30 941 kg	34 984 kg	35 054 kg
	Used fuel tank volume ratio	$V_{F,req}/V_F$	0.7913	0.8235	0.8342
	Angle of attack	α	2.8°	3.0°	2.5°
	Lift-to-drag ratio	L/D	17.55	18.31	18.37
	Center of pressure	$y_{CoP}/(b/2)$	0.3882	0.3864	0.3909
	Fuel consumption	$m_F/(R\,m_P)$	1.936×10^{-4} km^{-1}	1.658×10^{-4} km^{-1}	1.651×10^{-4} km^{-1}
Objective	Combined fuel consumption	$m_F/(R\,m_P)$	1.645×10^{-4} km^{-1}	1.496×10^{-4} km^{-1}	1.493×10^{-4} km^{-1}
	CO_2 emissions per passenger kilometres[b]	$m_{CO2}/(R\,m_P)$	54.4 g$_{CO2}$/pkm	49.5 g$_{CO2}$/pkm	49.4 g$_{CO2}$/pkm

[a] Values are scaled by a factor of 1.25 to account for additional masses of local reinforcements for load application and fasteners.
[b] Values of 3.15 kg$_{CO2}$/kg$_{Fuel}$ for a turbofan engine [53] and 105 kg for the passenger mass with baggage are assumed.

TAB 8. Results overview of wing optimization and recalculation with modified aerofoils.

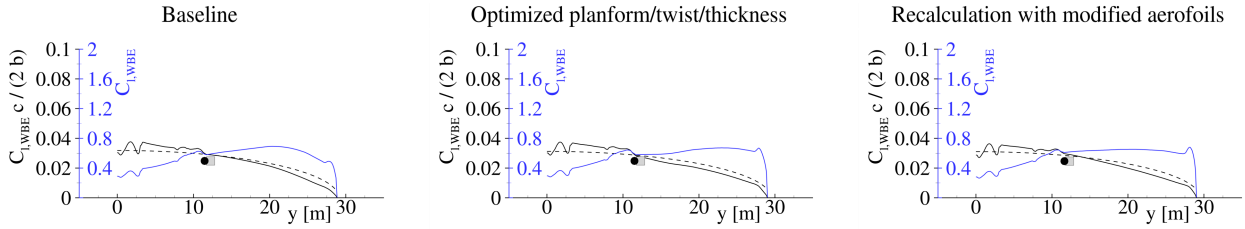

FIG 10. Lift and lift coefficient distributions for cruise flight of wing optimization with different aerofoils.

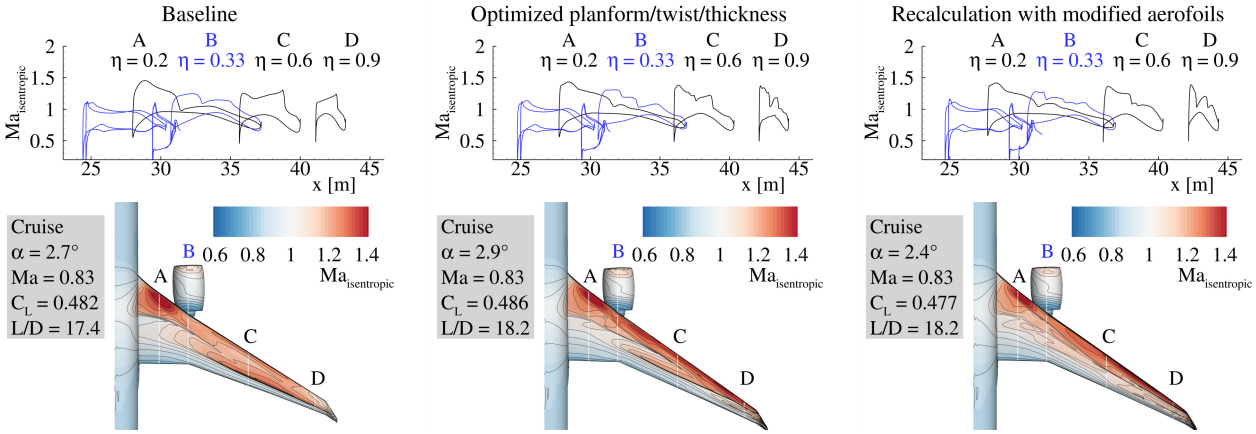

FIG 11. Isentropic Mach number distributions for upper wing surface of wing optimization with different aerofoils.

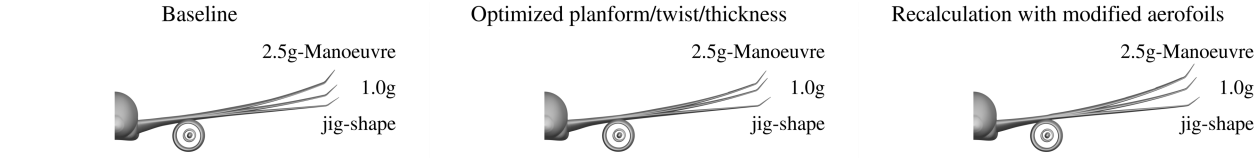

FIG 12. Wing deformations for cruise and manoeuvre flight of wing optimization with different aerofoils.

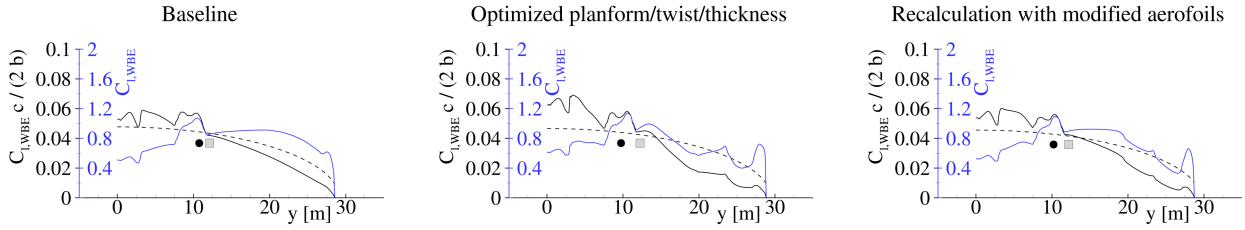

FIG 13. Lift and lift coefficient distributions for manoeuvre flight of wing optimization with different aerofoils.

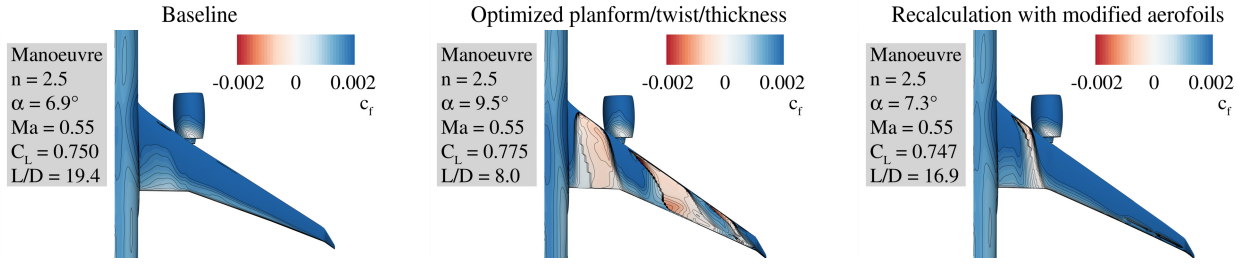

FIG 14. Skin friction distributions for manoeuvre flight of wing optimization with different aerofoils.

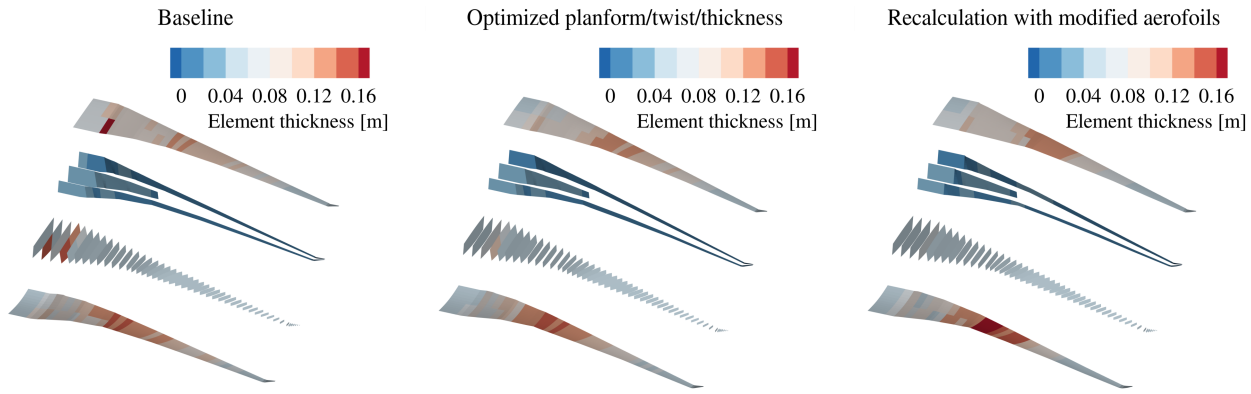

FIG 15. Wing box element thickness (skin thickness + stringer height) distributions of wing optimization with different aerofoils.

combination with the adapted aerofoil shapes and the relative aerofoil thickness to lower values for the isentropic Mach number in the inboard wing region (see FIG. 11). In the pull up manoeuvre, a significant inboard load shift occurs due to static aeroelastic effects of the backward swept wing [54, 55]. This inboard load shift is stronger for the optimized wing due to aileron deflections for manoeuvre load alleviation in comparison to baseline wing. Thereby, the inboard load shift is related to a forward shifting of the center of pressure in the case of backward swept wings and the aircraft trimming redistributes the lift between the wing and the horizontal tail. As a result, the lift of the horizontal tail increases and simultaneously the lift of the wing decreases.

The resulting wing deformations are presented in FIG. 12 for the cruise flight condition and the $2.5g$ symmetric pull up manoeuvre in comparison to the rigid "jig-shape". The optimized wing shows higher deflections due to the more flexible wing box structures, which result from the use of basic manoeuvre load alleviation functions and the reduced absolute wing thickness in the inboard wing region.

In FIG. 13 the lift distributions for the $2.5g$ symmetric pull up manoeuvre are presented. For each lift distribution the related elliptical lift distribution is shown by a dashed dotted line and the corresponding center of lift is indicated by a white rectangle as a reference. In the lift distribution of the optimized wing the aerodynamic effect of the aileron deflections can be observed in the outboard wing region. The center of lift is shifted inboard for the optimized wing in comparison to the baseline wing.

In FIG. 14 the corresponding skin friction distributions are shown for the $2.5g$ symmetric pull up manoeuvre. The skin friction distribution of the baseline wing indicates attached flow over the upper side of the wing. In contrast to the baseline wing, the wing optimization of the planform, twist and thickness leads to a wing shape, which shows massive flow separations on the upper side of the wing under manoeuvre flight conditions. On the basis of a conservative selection of the flight condition for the $2.5g$ symmetric pull up manoeuvre this result indicates an insufficient low speed flight performance in clean configuration. To improve the low speed flight performance in terms of maximal lift coefficient the aerofoils in the outboard wing region have been modified. These modified aerofoils have been designed with an inverse design method [56]. The prescribed target pressure distributions of this design method have a significantly reduced suction peak in the leading edge region and result in aerofoil shapes with increased leading edge radius. With the use of this modified aerofoils in the outboard wing region, the recalculation of the optimized wing shows predominantly attached flow under manoeuvre flight conditions as shown in FIG. 14. This indicates an improved low speed flight performance of the optimized wing with modified aerofoils.

In addition an overview of the structural results is presented in FIG. 15. The element thickness (sum of skin thickness and stringer height) distribution is shown for the spars, ribs and covers of the sized wing box.

The optimized wing and the recalculation with modified aerofoils show a similar thickness distribution. The upper and lower covers have the highest thickness of all components. Therefore, the covers have the biggest mass contribution. All results show a thickness peak at the engine position and the kink. Furthermore, the spars in the center wing region of the optimized wing are getting thinner due to the reduced aerofoil thickness and the corresponding reduction of buckling areas, where stability is still the sizing criteria for the spars. While optimizing the aerofoil thickness the thickness of the covers increase slightly with decreasing aerofoil thickness.

5. CONCLUSION AND OUTLOOK

In this work, the usage of an aero-structural wing optimization based on high fidelity simulation methods for the wing design of a highly efficient long-haul airliner has been successfully demonstrated. In order to find the optimum trade-off between aerodynamic performance and wing mass, the twist and thickness distribution and the wing planform design parameters have

been involved in the wing optimization. The results of this optimization show the expected reduction of the combined fuel consumption due to decreased wing mass based on active load distribution adaptation in manoeuvre flight and an increased aerodynamic performance under cruise flight conditions. This increase in aerodynamic performance has been achieved with slightly reduced wing area, increased wingspan, higher wing leading edge sweep angle and significant thinner inboard wing sections.

With the application of basic functions for manoeuvre load alleviation, the significance of aerodynamic loads redistribution has been shown. The structural wing sizing based on a reduced level of aerodynamic loads, results in a significant wing mass reduction and more wing flexibility.

Within the wing planform optimizations only 1 % of the wing geometries in the selected design space have fulfilled the geometrical constraints and have been considered in the aero-structural wing analysis. This observation shows the importance of the consideration of engine and landing gear integration and control surface constraints.

Another aspect of the wing optimization results obtained, is the observation of massive flow separations under manoeuvre flight conditions, which significantly influences the aerodynamic loads and indicates an insufficient low speed flight performance in clean configuration. These improper aerodynamic characteristics have been improved by modifying the aerofoils shapes. Thereby, the aerodynamic cruise flight performance and the wing mass could be maintained.

In the future, the aero-structural wing optimization have to be integrated into the complete aircraft design process. The aircraft design and optimization process has to be extended with engine design and integration and take-off and landing simulation capability based on high fidelity simulation methods. Furthermore, the integration of the aerofoil design and optimization process has to be improved under consideration of low speed flight performance constraints.

For the future design and optimization of the optimal load-adaptive aircraft in the DLR project oLAF, the aerodynamic limits of control surface effectiveness and load redistribution have to be predicted accurately to investigate the full potential of manoeuvre load reduction technology.

ACKNOWLEDGMENTS

The author would like to thank Andreas Schuster and Sascha Dähne from the DLR-Institute of Composite Structures and Adaptive Systems for providing the structure model generation tool and the structural analysis and sizing process to perform the aero-structural wing optimization presented in this publication. In addition, the author would like to thank Martin Kruse from the DLR-institute of Aerodynamics and Flow Technology for providing the aerofoils he designed.

Contact address:

tobias.wunderlich@dlr.de

References

[1] German Aerospace Center. *Towards zero-emission Aviation - How DLR's Aviation Research Strategy supports the European Green Deal 2050*. Cologne, Germany: German Aerospace Center (DLR), 2022. URL: https://www.dlr.de/content/en/downloads/publications/brochures/2021/towards-zero-emission-aviation.html.

[2] European Commision. *Sustainable and Smart Mobility Strategy*. Luxembourg, Belgium: Office for Official Publications of the European Communities, Dec. 2020. URL: https://ec.europa.eu/commission/presscorner/detail/en/fs_20_2350.

[3] G. W. K. Kenway and J. R. R. A. Martins. "High-fidelity aerostructural optimization considering buffet onset". In: *16th AIAA/ISSMO Multidisciplinary Analysis and Optimization Conference, Texas, USA*. June 2015. URL: https://doi.org/10.2514/6.2015-2790.

[4] R. J. White. "Improving the Airplane Efficiency by Use of Wing Maneuver Load Alleviation". In: *Journal of Aircraft* 8.10 (1971), pp. 769–775. URL: https://doi.org/10.2514/3.59169.

[5] G. E. Bendixen et al. "Digital active control system for load alleviation for the Lockheed L-1011". In: *The Aeronautical Journal* 85.849 (1981), pp. 430–436.

[6] C. D. Regan and C. V. Jutte. *Survey of Applications of Active Control Technology for Gust Alleviation and New Challenges for Lighter-weight Aircraft*. Tech. rep. NASA/TM-2012-216008. National Aeronautics and Space Administration, 2012.

[7] J. Xu and I. Kroo. "Aircraft Design with Active Load Alleviation and Natural Laminar Flow". In: *Journal of Aircraft* 51.5 (2014), pp. 1532–1545. URL: https://doi.org/10.2514/1.C032402.

[8] T. R. Brooks et al. "Aerostructural Tradeoffs for Tow-Steered Composite Wings". In: *Journal of Aircraft* 57.5 (2020), pp. 787–799. URL: https://doi.org/10.2514/1.C035699.

[9] R. G. Cook et al. "Industrially Inspired Gust Loads Analysis of Various-Aspect-Ratio Wings Featuring Geometric Nonlinearity". In: *Journal of Aircraft* 57.1 (2010), pp. 13–18. URL: https://doi.org/10.2514/1.C035294.

[10] V. Handojo et al. "Potential Estimation of Load Alleviation and Future Technologies in Reducing Aircraft Structural Mass". In: *Aerospace* 9.8 (2022). URL: https://doi.org/10.3390/aerospace9080412.

[11] S. Binder et al. "The interaction between active aeroelastic control and structural tailoring in aeroservoelastic wing design". In: *Aerospace Science and Technology* 110 (2021), p. 106516. URL: https://doi.org/10.1016/j.ast.2021.106516.

[12] T. F. Wunderlich et al. "Global aero-structural design optimization of composite wings with active manoeuvre load alleviation". In: *CEAS Aeronautical Journal* (May 2022). URL: https://doi.org/10.1007/s13272-022-00585-3.

[13] A. Jameson et al. "Multi-point Aero-Structural Optimization of Wings Including Planform Variations". In: *45th Aerospace Sciences Meeting and Exhibit, Reno, Nevada, USA*. AIAA 2007-764. 2007. URL: https://doi.org/10.2514/6.2007-764.

[14] J. R. R. A. Martins and J. T. Hwang. "Review and Unification of Methods for Computing Derivatives of Multidisciplinary Computational Models". In: *AIAA Journal* 51.11 (2013), pp. 2582–2599. URL: https://doi.org/10.2514/1.J052184.

[15] R. P. Liem et al. "Multimission Aircraft Fuel-Burn Minimization via Multipoint Aerostructural Optimization". In: *AIAA Journal* 53.1 (2015), pp. 104–122. URL: https://doi.org/10.2514/1.J052940.

[16] S. Keye et al. "Aero-Structural Optimization of the NASA Common Research Model". In: *18th AIAA/ISSMO Multidisciplinary Analysis and Optimization Conference*. AIAA 2017-4145. June 2017. URL: https://doi.org/10.2514/6.2017-4145.

[17] M. Abu-Zurayk et al. "Sensitivity-based Multifidelity Multidisciplinary Optimization of a Powered Aircraft Subject to a Comprehensive Set of Loads". In: *AIAA Aviation Forum 2020*. June 2020. URL: https://doi.org/10.2514/6.2020-3168.

[18] M. Schulze et al. "Aeroelastic Design of the oLAF Reference Aircraft Configuration". In: *Deutscher Luft- und Raumfahrtkongress (DLRK)*. Sept. 2021. URL: https://elib.dlr.de/143642/.

[19] C. M. Liersch and M. Hepperle. "A distributed toolbox for multidisciplinary preliminary aircraft design". In: *CEAS Aeronautical Journal* 2.1–4 (2011), pp. 57–68. URL: https://doi.org/10.1007/s13272-011-0024-6.

[20] B. Nagel et al. "Communication in Aircraft Design Can we Establish a Common Language". In: *28th Interantional Congress of the Aeronautical Sciences, ICAS 2012*. ICAS Conference Paper. Sept. 2012. URL: https://elib.dlr.de/134586.

[21] T. F. Wunderlich et al. "Multidisciplinary optimization of an NLF forward swept wing in combination with aeroelastic tailoring using CFRP". In: *CEAS Aeronautical Journal* 8.4 (2017), pp. 673–690. URL: https://doi.org/10.1007/s13272-017-0266-z.

[22] T. F. Wunderlich and L. Reimer. "Integrated Process Chain for Aerostructural Wing Optimization and Application to an NLF Forward Swept Composite Wing". In: *AeroStruct: Enable and Learn How to Integrate Flexibility in Design*. Ed. by R. Heinrich. Vol. 138. Notes on Numerical Fluid Mechanics and Multidisciplinary Design (NNFM). Cham: Springer International Publishing, 2018, pp. 3–33. URL: https://doi.org/10.1007/978-3-319-72020-3_1.

[23] J. R. R. A. Martins and A. B. Lambe. "Multidisciplinary Design Optimization: A Survey of Architectures". In: *AIAA Journal* 51.9 (2013), pp. 2049–2075. URL: https://doi.org/10.2514/1.J051895.

[24] T. F. Wunderlich et al. "Global Aero-Structural Design Optimization of More Flexible Wings for Commercial Aircraft". In: *AIAA Aviation Forum 2020*. June 2020. URL: https://doi.org/10.2514/6.2020-3170.

[25] A. B. Lambe and J. R. R. A. Martins. "Extensions to the Design Structure Matrix for the Description of Multidisciplinary Design Analysis and Optimization Processes". In: *Structural and Multidisciplinary Optimization* 46 (2012), pp. 273–284. URL: https://doi.org/10.1007/s00158-012-0763-y.

[26] A. Rempke. "Netzdeformation mit Elastizitätsanalogie in multidisziplinärer FlowSimulator-Umgebung". In: *20. DGLR - Fach - Symposium der STAB 2016*. Vol. 2016. 2016, pp. 128–129. URL: https://elib.dlr.de/109263.

[27] M. Meinel and G. O. Einarsson. "The FlowSimulator framework for massively parallel CFD applications". In: *PARA 2010 conference, 6-9 June, Reykjavik, Iceland*. 2010. URL: https://elib.dlr.de/67768.

[28] L. Reimer et al. "Multidisciplinary Analysis Workflow with the FlowSimulator". In: *Proceedings of the Onera Scientific Day 2012—CFD Workflow: Mesh, Solving, Visualizing, ...* Ed. by C. Benoit et al. Vol. 19. Amphithéâtre Becquerel, École Polytechnique, Palaiseau, 2012, pp. 23–30. URL: https://elib.dlr.de/78601.

[29] L. Reimer et al. "Towards Higher-Precision Maneuver and Gust Loads Computations of Aircraft: Status of Related Features in the CFD-Based Multidisciplinary Simulation Environment FlowSimulator". In: *New Results in Numerical and Experimental Fluid Mechanics XII*. Ed. by A. Dillmann et al. Cham: Springer International Publishing, 2020, pp. 597–607. URL: https://doi.org/10.1007/978-3-030-25253-3_57.

[30] T. Führer et al. "Automated model generation and sizing of aircraft structures". In: *Aircraft Engineering and Aerospace Technology* 88.2 (2016), pp. 268–276. URL: https://elib.dlr.de/103351.

[31] C. Geuzaine and J.-F. Remacle. "Gmsh: A 3-D finite element mesh generator with built-in pre- and post-processing facilities". In: *International Journal for Numerical Methods in Engineering* 79.11 (2009), pp. 1309–1331. URL: https://onlinelibrary.wiley.com/doi/abs/10.1002/nme.2579.

[32] R. Kamakoti and W. Shyy. "Fluid-structure interaction for aeroelastic applications". In: *Progress in Aerospace Sciences* 40.8 (2005), pp. 535–558. URL: http://www.sciencedirect.com/science/article/pii/S0376042105000084.

[33] X. B. Lam et al. "Coupled Aerostructural Design Optimization Using the Kriging Model and Integrated Multiobjective Optimization Algorithm". In: *Journal of Optimization Theory and Applications* 142.3 (2009), pp. 533–556. URL: https://doi.org/10.1007/s10957-009-9520-9.

[34] T. Gerhold. "Overview of the Hybrid RANS TAU-Code". In: *MEGAFLOW - Numerical Flow Simulation for Aircraft Design*. Ed. by N. Kroll and J. K. Fassbender. Vol. 89. Berlin, Heidelberg: Springer Berlin Heidelberg, 2005, pp. 81–92. URL: https://doi.org/10.1007/3-540-32382-1_5.

[35] D. Schwamborn et al. "The DLR TAU-Code: Recent Applications in Research and Industry". In: *European Conference on Computational Fluid Dynamics, ECCOMAS CFD 2006 Conference, Delft, The Netherlands*. 2006. URL: https://elib.dlr.de/22421.

[36] E. N. Tinoco et al. “Summary Data from the Sixth AIAA CFD Drag Prediction Workshop: CRM Cases”. In: *Journal of Aircraft* 55.4 (2018), pp. 1352–1379. URL: https://doi.org/10.2514/1.C034409.

[37] S. Dähne et al. “Steps to Feasibility for Laminar Wing Design in a Multidisciplinary Environment”. In: *29th Congress of the International Council of the Aeronautical Sciences, ICAS 2014*. Sept. 2014. URL: https://elib.dlr.de/90644.

[38] H. Barnewitz and B. Stickan. “Improved Mesh Deformation”. In: *Management and Minimisation of Uncertainties and Errors in Numerical Aerodynamics: Results of the German collaborative project MUNA*. Ed. by B. Eisfeld et al. Vol. 122. Berlin, Heidelberg, 2013, pp. 219–243. URL: https://doi.org/10.1007/978-3-642-36185-2_9.

[39] G. A. Wilke. “Variable-Fidelity Methodology for the Aerodynamic Optimization of Helicopter Rotors”. In: *AIAA Journal* 57.8 (2019), pp. 3145–3158. URL: https://doi.org/10.2514/1.J056486.

[40] D. R. Jones et al. “Efficient Global Optimization of Expensive Black-Box Functions”. In: *Journal of Global Optimization* 13.4 (1998), pp. 455–492. URL: https://doi.org/10.1023/A:1008306431147.

[41] A. Forrester et al. *Engineering Design via Surrogate Modelling: A Practical Guide*. Wiley, 2008. URL: https://doi.org/10.1002/9780470770801.

[42] L. Ju et al. “Probabilistic methods for centroidal Voronoi tessellations and their parallel implementations”. In: *Parallel Computing* 28.10 (2002), pp. 1477–1500. URL: https://doi.org/10.1016/S0167-8191(02)00151-5.

[43] D. G. Krige. “A Statistical Approach to Some Basic Mine Valuation Problems on the Witwatersrand”. In: *Journal of the Chemical, Metallurgical and Mining Society of South Africa* 52.6 (Dec. 1951), pp. 119–139. URL: http://doi.org/10.2307/3006914.

[44] R. Storn and K. Price. “Differential Evolution - A Simple and Efficient Heuristic for global Optimization over Continuous Spaces”. In: *Journal of Global Optimization* 11.4 (1997), pp. 341–359. URL: https://doi.org/10.1023/A:1008202821328.

[45] J. A. Nelder and R. Mead. “A Simplex Method for Function Minimization”. In: *Computer Journal* 7 (1965), pp. 308–313.

[46] J. Roskam. *Airplane Design Part 1: Preliminary Sizing of Airplanes*. Lawrence, Kansas, USA: Design, Analysis and Research Corporation, 120 East Ninth Street, Suite 2, Lawrence, Kansas, 66044, USA, 1989.

[47] D. P. Raymer. *Aircraft Design: A Conceptual Approach*. Third Edition. AIAA education series. American Institute of Aeronautics and Astronautics, 1999.

[48] L. R. Jenkinson et al. *Civil Jet Aircraft Design*. AIAA education series. American Institute of Aeronautics and Astronautics (AIAA), 1999. URL: https://doi.org/10.2514/4.473500.

[49] J. D. Mattingly et al. *Aircraft Engine Design*. Second Edition. American Institute of Aeronautics and Astronautics, 2002. URL: https://doi.org/10.2514/4.861444.

[50] L. M. Nicolai and G. Carichner. *Fundamentals of Aircraft and Airship Design*. Vol. 1. AIAA education series. American Institute of Aeronautics and Astronautics, 2010. URL: https://doi.org/10.2514/4.867538.

[51] D. P. Raymer. *Aircraft Design: A Conceptual Approach*. Sixth Edition. AIAA education series. American Institute of Aeronautics and Astronautics, 2019. URL: https://doi.org/10.2514/4.105746.

[52] M.-H.-1.-3. Military. *Composite Materials Handbook, Polymer Matrix Composites: Materials Usage, Design, and Analysis*. Vol. 3 of 5. US Department of Defense, June 2002.

[53] N. E. Antoine and I. M. Kroo. “Aircraft Optimization for Minimal Environmental Impact”. In: *Journal of Aircraft* 41.4 (2004), pp. 790–797. URL: https://doi.org/10.2514/1.71.

[54] T. F. Wunderlich. “Multidisziplinäre Optimierung von Flügeln für Verkehrsflugzeuge mit Berücksichtigung der statischen Aeroelastizität”. PhD thesis. Technische Universität Braunschweig, Mar. 2013. URL: https://elib.dlr.de/88002.

[55] T. F. Wunderlich. “Multidisciplinary wing optimization of commercial aircraft with consideration of static aeroelasticity”. In: *CEAS Aeronautical Journal* 6.3 (2015), pp. 407–427. URL: https://doi.org/10.1007/s13272-015-0151-6.

[56] W. Bartelheimer. “An inverse method for the design of transonic airfoils and wings”. In: *Inverse Problems in Engineering* 4 (1996), pp. 21–51.